Dynamic Analysis of Dual-Mesh Parallel Axis Spur Gear Systems

Undergraduate Thesis

The Ohio State University
Department of Mechanical and Aerospace Engineering
April 2014

John Anthony Scheick
scheick.3@osu.edu
Advisor: Dr. Rajendra Singh
Co-Advisor: Dr. Jason Dreyer

Committee:

R. Singh, Mechanical and Aerospace Engineering, singh.3@osu.edu

J. Dreyer, Mechanical and Aerospace Engineering, dreyer.24@osu.edu

K. Srinivasan, Mechanical and Aerospace Engineering, srinivasan.3@osu.edu

Presented in Partial Fulfillment of the

Requirements for Graduation with Research Distinction

In the Department of Mechanical Engineering at

The Ohio State University

Abstract

This research investigates the vibration characteristics of two dual-mesh parallel axis spur gear systems based on the linear time-invariant system theory. Conceptual analytical models are developed, which include elements of gear mesh stiffness, sliding friction, bearing stiffness, and torsional inertia. The first system includes three gears, each on its own shaft; the second system includes four gears with the middle two gears connected by a compliant shaft. The parameters for these studies are consistent with those previously used in models of a single-mesh system. The assumed excitations at the gear meshes are from static transmission error acting in the line-of-action direction and from sliding friction acting in the off-line-of-action direction. The natural frequencies and mode shapes for two configurations are compared to a single mesh system, and relevant modes are identified. In addition, the dynamic mesh force and dynamic bearing force spectra (for given excitations) are calculated for the dual-mesh systems and their sensitivities to changes of system parameters and excitation levels are investigated.

Table of Contents

Acknowledgements

I would like to thank all of the individuals that have provided support and guidance over the course of this project. I would like to acknowledge Dr. Rajendra Singh, Dr. Jason Dreyer and Dr. Krishnaswamy Srinivasan for their service in my defense committee and the guidance and critique they offered. I would like to thank Sriram Sundar for his guidance on my research as well as his help on creating the models. Finally, a special thanks to The College of Engineering at The Ohio State University for the financial support awarded during the duration of this project.

Vita

2009.....**Centerville High School, Centerville, OH**

Fields of Study

Major Field: Mechanical Engineering

List of Figures

List of Tables

Chapter 1: Introduction

1.1 Motivation/Literature Review

Multi-mesh, parallel axis geared systems are commonly found in applications ranging from automotive transmissions to helicopter drive trains and industrial gearboxes [1]. It is well known that gearboxes can produce extremely high levels of noise and vibrations; therefore, gear system dynamics research is focused on reducing these high levels of noise and vibrations. In a geared system, there are several sources of noise produced in a system, which can manifest under different operating conditions. Some of these sources include, but are not limited to, air trapped between the rotating gears, backlash, sliding friction of the gear teeth, and transmission error (the deviation from perfect conjugate motion of the gears), surface profile undulations, and gear spacing errors. This work will assume that sliding friction and transmission error are the main exciters of gear vibrations within the loaded gear pairs (no loss of contact). To minimize such sources of vibration and noise, it is necessary to understand the dynamic loads within the geared system at the design stage. While the dynamic behavior of single-mesh spur gear systems is a well-documented area [1], there are fewer publications on multi-mesh parallel axis spur gear systems [2]. Therefore, this thesis will develop simple illustrative models that will examine dynamic interactions between multiple gear meshes.

For this research, two different configurations of multi-mesh parallel axis spur gear systems will be modeled. The first system will have three gears, each on

its own shaft, as illustrated in Figure 1.1. The second system, also illustrated in Figure 1.1, has four gears with the middle two gears sharing a compliant shaft.

Figure 1.1: Representative Sketch of Three Gear System (Left) and Four Gear System (Right)

Once a proper analytical model for these two architectures is developed, suitable parameters for each are chosen. These parameters are chosen to be consistent with those previously used in models of a single-mesh system and the gear mesh stiffness values and the static transmission error come from a contact mechanics code, Load Distribution Program [3]. Two different forces excite the models at the gear meshes: a normal force generated from the static transmission error (STE) acting across the mesh stiffness in the Line-Of-Action (LOA) direction and a resulting sliding friction force acting in the Off-Line-Of-Action (OLOA) direction. Input or output torque fluctuations are not considered as excitations in this study. Figure 1.2 shows the path of the excitation sources in the models. The equations of motions with these excitations are solved numerically in MATLAB.

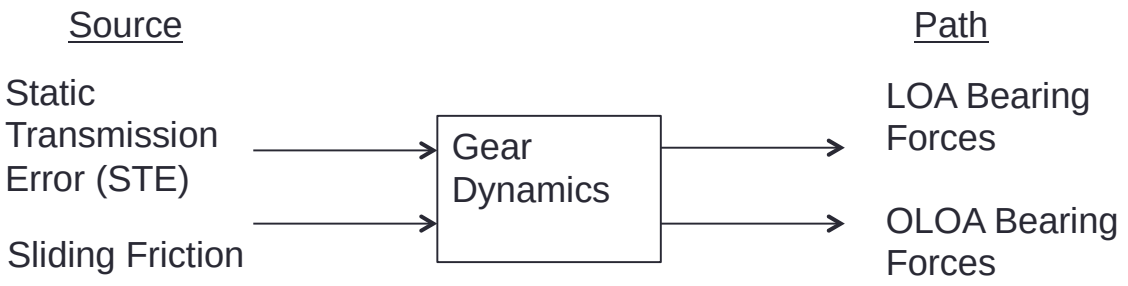

Figure 1.2 Gear Noise Sources and Paths

The models for each system are used to calculate the natural frequencies, mode shapes, dynamic bearing forces, and dynamic mesh forces of each of gear mesh. Having these responses of the two different architectures allows for a detailed comparison of how they compare under similar loaded conditions. In addition to comparing the two architectures, each individual system is analyzed to see how individual parameters affect these overall responses of the system; in this case, the bearing stiffness, static transmission error, damping ratio, and coefficient of friction are considered.

A similar model of a single mesh spur gear system containing 8 degrees of freedom was developed by Singh and Houser [1]. Comparisons to this single mesh gear system will be made to the two dual-mesh models developed in this paper.

1.2 Research Objectives

The objectives of this research are developed in order to isolate and compare the fundamental physical phenomena that differentiate the response of two different architectures of a dual-mesh gear system. This is to be accomplished by designing an analytical model of each of the two dual-mesh systems. The main

outcomes of this work are analytical models of the two systems that are used in several conceptual studies. The specific goals of this project are as follows:

i) Develop analytical linear system models of two dual-mesh spur gear systems.

ii) Compare the natural frequencies, mode shapes, dynamic bearing force and dynamic mesh force for a single mesh and two dual-mesh models.

iii) For the dual-mesh systems, quantify the dynamic bearing force spectra (with assumed coefficient of friction and static transmission error) given key parameters (bearing-shaft stiffness, damping ratio, coefficient of friction and static transmission error).

Chapter 2: Problem Formulation

2.1 Introduction

In this chapter, 11 and 14 degree-of-freedom linear-time-invariant (LTI) models of internal geared systems are developed. The systems are parallel axis multi-mesh spur gear systems, as described earlier. The dynamic behaviors of the systems are modeled in the frequency domain. A linear-time-invariant model of a single mesh gear system is also included for comparison.

2.2 Scope and Assumptions

A linear-time-invariant (LTI) model is developed for each of the simplified gear systems shown in Figure 2.2 and Figure 2.3. These are illustrative models of the systems with the excitation forces acting on both gears at each mesh. In the model formulations, each of the pinions and gears are assumed to be rigid disks. Elastic deformations of the shafts and bearings are modeled using a lump sum representation of their compliance in both the LOA and OLOA directions. Therefore, the bending modes of the shafts are not considered. In addition, the case or housing is considered to be rigid ground.

In the LOA, the primary excitation for a spur gear pair is the relative displacement at the gear mesh. This displacement is defined as the static transmission error or STE, $\epsilon(t)$. In an actual system, the STE is defined only at frequencies corresponding to the mesh harmonics. However, in order to simplify the problem, the STE is assumed to be the same amplitude for all the frequencies

considered in this study (10 to 20,000 Hz). In gear sets with a non-integer contact ratio, the number of teeth in contact changes throughout the mesh cycle. Inclusion of these time-varying parameters leads to a nonlinear governing equation. To develop a LTI model, an average number of teeth in contact is assumed and the mesh stiffness parameter is time averaged. The excitation force due to the STE (acting normal to the contact surfaces of the teeth, in the LOA) can be determined by the following equation where k_m is the mesh stiffness.

$$F_n = k_m \epsilon \tag{2.1}$$

The friction force, F_f, due to the sliding between mating gear teeth is the main excitation in the OLOA direction. To simplify the problem, this friction force is assumed to act externally on the gear pair. Just like the STE, the friction excitation is assumed to be constant across the entire frequency range with a coefficient of 0.03 (later varied in sensitivity studies). The excitation force due to the sliding friction (at the gear mesh in the OLOA direction) can be determined by the following equation, where μ is the coefficient of friction,

$$F_f = \mu F_n \tag{2.2}$$

2.3 11 Degree-of-Freedom LTI Model for Three Spur Gears (Model B)

A spur-geared system with 11 degrees-of-freedom (DOF), Model B, is shown below in Figure 2.2. The system consists of three gears, one pinion and two gears, each on their own shaft and bearing. The pinion, gear one and gear two each have a translational motion in the LOA and OLOA and one angular motion about each gear's axis of rotation. The translational motion in the LOA is denoted by x_p, x_{g1} and x_{g2}

and the translational motion in the OLOA is denoted by y_p, y_{g1} and y_{g2} where the subscript p refers to the pinion, g1 refers to first gear and g2 refers to second gear. The angular motion is denoted by θ_p, θ_{g1} and θ_{g2} for each of the gears. Figure 2.1 shows a representation of the dynamics of the gears on a single spur gear mesh for simplicity. The inertias and base radii for the pinion and gears are given by J_p, R_p, J_{g1}, R_{g1}, J_{g2} and R_{g2}, respectively, with the mesh stiffness denoted by K_m. The masses m_p, m_{g1} and m_{g2} represent the mass of the pinion and gears in addition to the mass contributed from the respective shafts. The inertias from the motor and load, J_d and J_L, are included to give more realistic boundary conditions. The shafts are modeled as simply supported beams, in which the shaft stiffness and bearing stiffness are combined in series to form an equivalent term, denoted as K_{px}, K_{g1x} and K_{g2x} for the LOA and K_{py}, K_{g1y} and K_{g2y} for the OLOA. The torsional shaft stiffness of the corresponding input and output shaft are given as K_{Td} and K_{TL}. The specific values for these parameters are detailed in Chapter 3.

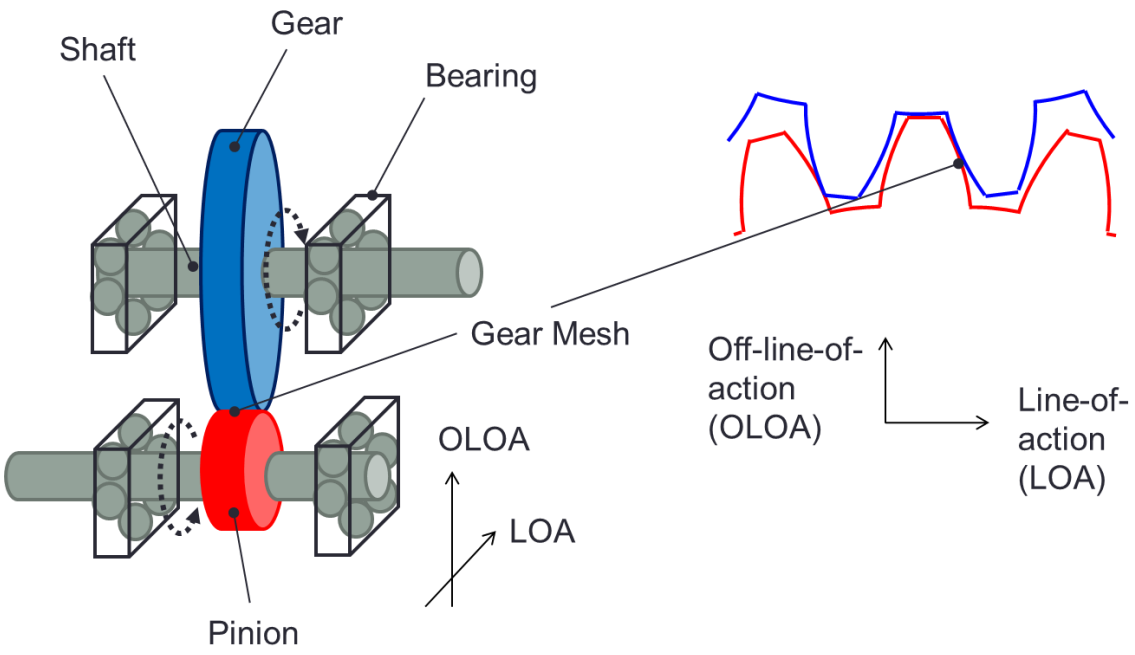

Figure 2.1: Gear Dynamics for a Single Gear Mesh

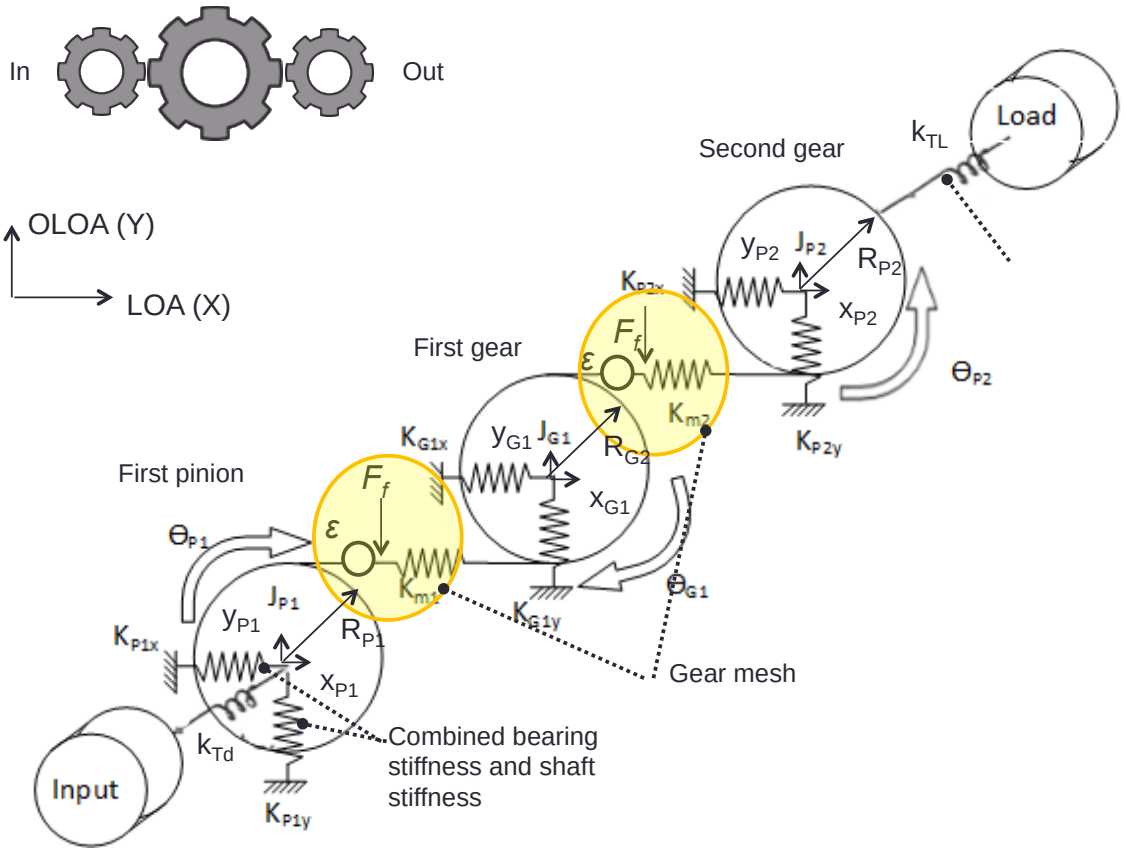

Figure 2.2: Schematic of the 11 DOF System (Model B)

2.4 Eigenvalue and Forced Vibration Problems

Newton's second law is used to formulate the equations of motion for these two systems. This results in n differential equations for each system, where n is the number of degrees-of-freedom of the system. Equation 2.3 gives the equation of motion for the system.

$$\mathbf{M}\{\ddot{\mathbf{q}}\} + \mathbf{C}\{\dot{\mathbf{q}}\} + \mathbf{K}\{\mathbf{q}(t)\} = \mathbf{F}(t) \quad (2.3) \qquad (2.3)$$

In Equation 2.3 **M** and **K** are the mass and stiffness matrices, respectively, **F** is the force vector, and ***q*** is the displacement vector, which can be defined as follows for Model B, for harmonic motion (at frequency ω in rad/s). The construction of the damping matrix, **C**, is detailed later in this section

$$\boldsymbol{M} = \left[diag\left(J_{p1}\ J_{g1}\ m_{p1}\ m_{g1}\ m_{p1}\ m_{g1}\ J_{g2}\ m_{g2}\ m_{g2}\ J_d\ J_L\right)\right] \quad (2.4)$$

$$\boldsymbol{K} = (\text{below}) \quad (2.5)$$

$$\begin{bmatrix}
R_{p1}^2 k_{m1} + k_{td} & -R_{p1}R_{g1}k_{m1} & R_{p1}k_{m1} & -R_{p1}k_{m1} & 0 & 0 & 0 & 0 & 0 & k_{td} & 0 \\
-R_{p1}R_{g1}k_{m1} & R_{g1}^2 k_{m1} + R_{g1}^2 k_{m2} & -R_{g1}k_{m1} & R_{g1}k_{m1} - R_{g1}k_{m2} & 0 & 0 & -R_{g1}R_{g2}k_{m2} & R_{g1}k_{m2} & 0 & 0 & 0 \\
R_{p1}k_{m1} & -R_{g1}k_{m1} & k_{p1x} + k_{m1} & -k_{m1} & 0 & 0 & 0 & 0 & 0 & 0 & 0 \\
-R_{1p}k_{m1} & R_{g1}k_{m1} - R_{g1}k_{m2} & -k_{m1} & k_{g1x} + k_{m1} + k_{m2} & 0 & 0 & R_{g2}K_{m2} & -k_{m2} & 0 & 0 & 0 \\
0 & 0 & 0 & 0 & k_{p1y} & 0 & 0 & 0 & 0 & 0 & 0 \\
0 & 0 & 0 & 0 & 0 & k_{g1y} & 0 & 0 & 0 & 0 & 0 \\
0 & -R_{g1}R_{g2}k_{m2} & 0 & R_{g2}k_{m2} & 0 & 0 & R_{g2}^2 k_{m2} + k_{tl} & -R_{g2}k_{m2} & 0 & 0 & -k_{tl} \\
0 & R_{g1}k_{m1} & 0 & -k_{m2} & 0 & 0 & -R_{g2}k_{m2} & k_{g2x} + k_{m2} & 0 & 0 & 0 \\
0 & 0 & 0 & 0 & 0 & 0 & 0 & 0 & k_{g2y} & 0 & 0 \\
-k_{tf} & 0 & 0 & 0 & 0 & 0 & 0 & 0 & 0 & k_{td} + k_a & 0 \\
0 & 0 & 0 & 0 & 0 & 0 & -k_{tl} & 0 & 0 & 0 & k_{tl} + k_a
\end{bmatrix}$$

$$\boldsymbol{F}(t) = \left[R_{p1}F_r + k_{m1}R_{p1}\varepsilon\ , -2R_{g1}F_r - 2k_{m1}R_{g1}\varepsilon\ ,\ k_{m1}\varepsilon\ ,\ 0\ ,\ -F_r\ , 0\ , R_{g2}F_r + k_{m2}R_{g2}\varepsilon\ , -k_{m2}\varepsilon\ , F_r\ , 0\ , 0\right]^T e^{j\omega t} \quad (2.6)$$

$$\boldsymbol{q}(t) = \left[\theta_{p1}\ \theta_{g1}\ x_{p1}\ x_{g1}\ y_{p1}\ y_{g1}\ \theta_{g2}\ x_{g2}\ y_{g2}\ \theta_d\ \theta_L\right]^T e^{j\omega t} \quad (2.7)$$

Assuming a proportionally damped system, to determine the natural frequencies of the models, the homogenous, undamped form of the system equation is needed. The homogenous form is given by Equation 2.8.

$$(-\omega^2 \boldsymbol{M} + \boldsymbol{K})\{\boldsymbol{q}\}e^{j\omega t} = 0 \tag{2.8}$$

Solving the homogenous form using the eigenvalue problem gives the following, where ω_i is the natural frequency of the system (in rad/s) and $\{\boldsymbol{q}\}_i$ is the corresponding mode shape to the natural frequency.

$$\omega_i^2 \boldsymbol{M}\{\boldsymbol{q}\}_i = \boldsymbol{K}\{\boldsymbol{q}\}_i \qquad i = 1,2,\cdots,n \tag{2.9}$$

For the forced vibration problem, a damping matrix with assumed modal damping is defined as

$$\boldsymbol{C} = [\boldsymbol{Q}^T]^{-1}\begin{bmatrix} \ddots & & \\ & 2\xi_i\omega_i & \\ & & \ddots \end{bmatrix}[\boldsymbol{Q}]^{-1} \tag{2.10}$$

where ω_i is the ith natural frequency, ξ_i is the damping ratio associated with the ith mode and $\boldsymbol{Q} = [\{\boldsymbol{q}\}_1\ \{\boldsymbol{q}\}_2\ \ldots\ \{\boldsymbol{q}\}_n]$ which is a matrix comprised of all the modes shapes of the system. Then, the motion vector of the system under a given harmonic load vector is given by

$$\{\boldsymbol{q}(\omega)\} = [-\omega^2 \boldsymbol{M} + j\omega \boldsymbol{C} + \boldsymbol{K}]^{-1}\boldsymbol{F} \tag{2.11}$$

For a given frequency, ω, the bearing force in the LOA direction on the pinion can be determined by

$$F_{px}(\omega) = (j\omega c_{px} + k_{px})x_p(\omega) \tag{2.12}$$

where x_p is the LOA pinion displacement in the calculated motion vector $\{\boldsymbol{q}(\omega)\}$, k_{px} and c_{px} are the stiffness and damping parameters associated with the pinion

support stiffness in the LOA direction. The bearing force in the OLOA direction is determined by

$$F_{py}(\omega) = (j\omega c_{py} + k_{py}) y_p(\omega) \tag{2.13}$$

where y_p is the OLOA pinion displacement in the calculated motion vector $\{\boldsymbol{q}(\omega)\}$, k_{py} and c_{py} are the stiffness and damping parameters associated with the pinion support stiffness in the OLOA direction. The dynamic bearing force magnitude at the pinion is then assumed as

$$F_p(\omega) = \sqrt{(F_{px}(\omega))^2 + (F_{py}(\omega))^2} \tag{2.14}$$

For the calculation of the dynamic mesh force, the dynamic transmission error (DTE) is needed. For a given frequency, ω, the DTE at a gear-pinion interface is given by

$$\delta(\omega) = R_p \theta_p(\omega) + x_p(\omega) - R_g \theta_g(\omega) + x_g(\omega) \tag{2.15}$$

where the subscript p refers to the pinion and g refers to the gear and θ and x are displacements in the calculated motion vector in Equation 2.11. The dynamic mesh force at the gear-pinion interface is then

$$F_m(\omega) = (j\omega c_m + k_m)(\delta(\omega) - \varepsilon(\omega)) \tag{2.16}$$

where ε is the STE and k_m and c_m are the stiffness and damping parameters associated with the gear mesh.

2.5 14 Degree-of-Freedom LTI Model for Four Spur Gears (Model C)

A similar methodology to that described in Section 2.3 is followed for the development of a 14 DOF LTI model, Model C. The schematic for Model C is shown in

Figure 2.3. Here, the drive and load gear are connected by two intermediate gears sharing a compliant shaft instead of a single gear. Again, each of the gears has two translational motions, x_{p1}, y_{p1}, x_{g1}, y_{g1}, x_{p2}, y_{p2}, x_{g2}, y_{g2}, one in the LOA (x) and one in the OLOA (y). Here the subscript p1 represents the first pinion, the driven gear, g1 denotes the first intermediary gear, p2 denotes the second intermediary gear and g2 denotes the final gear, the load gear. In addition to the translational motion, each gear has one vibratory angular motion about the gear's axis, θ_{p1}, θ_{g1}, θ_{p2} and θ_{g2}. The base radii and inertias for each of the gears are given respectively by R_{p1}, J_{p1}, R_{g1}, J_{g1}, R_{p2}, J_{p2}, R_{g2} and J_{g2}. The driving motor and load are also given inertia, J_d and J_L to create more realistic boundary conditions. The torsional shaft stiffness of the corresponding input, intermediate and output shafts are given as K_{td}, K_t and K_{tL} with the mesh stiffness represented by K_{m1} and K_{m2} for the first and second meshes. As before, the mesh stiffness is assumed to be time-averaged. The terms m_{p1}, m_{g1}, m_{p2} and m_{g2} represent the mass of the four gears along with the contribution from the respective shafts. The shafts are modeled as simply supported beams in both the LOA and OLOA directions, with an effective bearing-shaft stiffness of K_{xp1}, K_{yp1}, K_{xg1}, K_{yg1}, K_{xp2}, K_{yp2}, K_{xg2} and K_{yp2} for each of the gears.

The excitations of the system come from the STE displacement, $\varepsilon(t)$, at the gear mesh in the LOA direction and the friction force, F_f, due to the sliding of mating gear teeth in the OLOA direction. Just as in the previous section, both excitations are assumed to have constant amplitude over the entire frequency range.

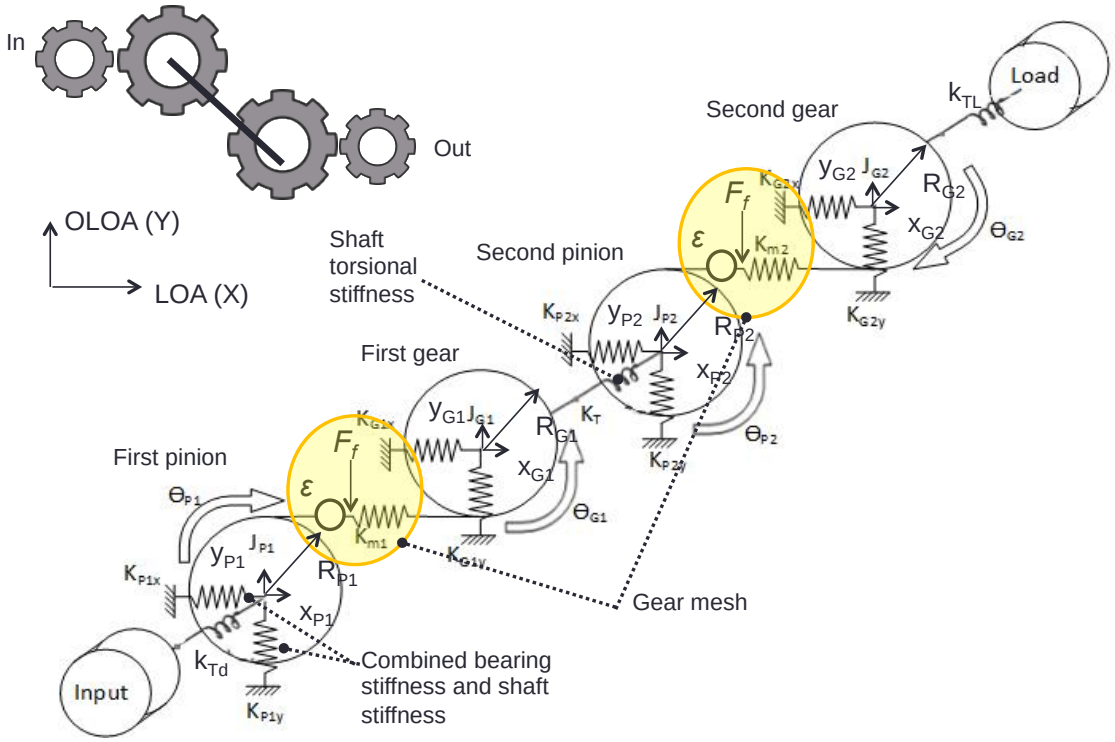

Figure 2.3: Schematic of the 14 DOF System (Model C)

2.6 Equations of Motion for 14 DOF System (Model C)

Just as in section 2.4, Model C is modeled using Newton's Laws yielding Equation 2.3, given below for reference.

$$\mathbf{M}\{\ddot{\mathbf{q}}\}+\mathbf{C}\{\dot{\mathbf{q}}\}+\mathbf{K}\{\mathbf{q}(t)\}=\mathbf{F}(t) \quad (2.3) \qquad (2.3)$$

Here **M** and **K** are the mass and stiffness matrices, respectively, **F** is the force vector, and ***q*** is the displacement vector, which can be defined as follows for Model C, for harmonic motion. The construction of the damping matrix, **C**, follows the same process as in Section 2.4.

$$\boldsymbol{M} = \left[diag\left(J_d \;\; m_{p1} \;\; m_{p1} \;\; J_{p1} \;\; J_{g1} \;\; m_{g1} \;\; m_{g1} \;\; m_{p2} \;\; m_{p2} \;\; J_{p2} \;\; J_{g2} \;\; m_{g2} \;\; m_{g2} \;\; J_L\right)\right] \quad (2.17)$$

$$\boldsymbol{K} = \text{(below)} \quad (2.18)$$

$$\begin{bmatrix}
k_{td}+k_a & 0 & 0 & -k_{td} & 0 & 0 & 0 & 0 & 0 & 0 & 0 & 0 & 0 & 0 \\
0 & k_{p1y} & 0 & 0 & 0 & 0 & 0 & 0 & 0 & 0 & 0 & 0 & 0 & 0 \\
0 & 0 & k_{p1x}+k_{m1} & R_{p1}k_{m1} & -R_{g1}k_{m1} & -k_{m1} & 0 & 0 & 0 & 0 & 0 & 0 & 0 & 0 \\
-k_{td} & 0 & R_{p1}k_{m1} & R_{p1}^2k_{m1}+k_{td} & -R_{p1}R_{g1}k_{m1} & -R_{p1}k_{m1} & 0 & 0 & 0 & 0 & 0 & 0 & 0 & 0 \\
0 & 0 & -R_{g1}k_{m1} & -R_{p1}R_{g1}k_{m1} & R_{g1}^2k_{m1}+k_{tran} & R_{g1}k_{m1} & 0 & 0 & 0 & -k_{tran} & 0 & 0 & 0 & 0 \\
0 & 0 & -k_{m1} & -R_{p1}k_{m1} & R_{g1}k_{m1} & R_{g1x}+k_{m1} & 0 & 0 & 0 & 0 & 0 & 0 & 0 & 0 \\
0 & 0 & 0 & 0 & 0 & 0 & k_{g1y} & 0 & 0 & 0 & 0 & 0 & 0 & 0 \\
0 & 0 & 0 & 0 & 0 & 0 & 0 & k_{p2y} & 0 & 0 & 0 & 0 & 0 & 0 \\
0 & 0 & 0 & 0 & 0 & 0 & 0 & 0 & k_{p2x}+k_{m2} & R_{p2}k_{m2} & -R_{g2}k_{m2} & -k_{m2} & 0 & 0 \\
0 & 0 & 0 & 0 & -k_{tran} & 0 & 0 & 0 & R_{p2}k_{m2} & R_{p2}^2k_{m2}+k_{tran} & -R_{p2}R_{g2}k_{m2} & -R_{p2}k_{m2} & 0 & 0 \\
0 & 0 & 0 & 0 & 0 & 0 & 0 & 0 & -R_{g2}k_{m2} & -R_{p2}R_{g2}k_{m2} & R_{g2}^2k_{m2}+k_{tl} & R_{g2}k_{m2} & 0 & -k_{tl} \\
0 & 0 & 0 & 0 & 0 & 0 & 0 & 0 & -k_{m2} & -R_{p2}k_{m2} & R_{g2}k_{m2} & k_{g2x}+k_{m2} & 0 & 0 \\
0 & 0 & 0 & 0 & 0 & 0 & 0 & 0 & 0 & 0 & 0 & 0 & k_{g2y} & 0 \\
0 & 0 & 0 & 0 & 0 & 0 & 0 & 0 & 0 & 0 & -k_{tl} & 0 & 0 & k_{tl}+k_a
\end{bmatrix}$$

$$\boldsymbol{F}(t) = \left[0\,,-F_r\,,k_m\varepsilon\,,R_{p1}F_r+k_mR_{p1}\varepsilon\,,-R_{g1}F_r-k_mR_{g1}\varepsilon\,,-k_m\varepsilon\,,F_r\,,F_r\,,-k_mE\,,R_{p1}F_r+k_mR_{p2}\varepsilon\,,-R_{g3}F_r-k_mR_{g2}\varepsilon\,,\right.$$

$$\left.k_m\varepsilon\,,-F_r\,,0\right]^T e^{j\omega t} \quad (2.19)$$

$$\boldsymbol{q}(t) = \left[\theta_d \;\; y_{p1} \;\; x_{p1} \;\; \theta_{p1} \;\; \theta_{g1} \;\; x_{g1} \;\; y_{g1} \;\; y_{p2} \;\; x_{p2} \;\; \theta_{p2} \;\; \theta_{g2} \;\; x_{g2} \;\; y_{g2} \;\; \theta_L\right]^T e^{j\omega t} \quad (2.20)$$

Following the same process in Section 2.4, the natural frequencies of Model C can be obtained using Equation 2.9, the dynamic bearing force can be determined with Equation 2.14 and the dynamic mesh force can be determined with Equation 2.16. Again, these parameters are detailed in Chapter 3.

2.7 Single Mesh Model with Two Spur Gears (Model A)

An 8 degree-of-freedom model, Model A, of a single gear mesh with two spur gears is used to provide context for the responses of the two dual-mesh models. This model, as depicted in Figure 2.4, is developed with the same assumptions as Models B and C as denoted in Sections 2.3 and 2.5. Model A consists of two spur gears in mesh, the drive gear, p, and the load gear, g. Both gears have two translational motions, x_p, y_p, x_g, y_g, one in the LOA (x) and one in the OLOA (y). Each gear has a vibratory angular motion about its axis of rotation, θ_p and θ_g. The base radii and inertias for the two gears are denoted by R_p, J_p, R_g, and J_g. The driving motor and load are given inertia and torsional stiffness, J_d, k_{td}, J_L and k_{tl} to create a more realistic boundary condition. The terms m_p and m_g represent the mass of the two gears along with the contribution from the respective shafts. The shafts are modeled as simply supported beams in both the LOA and OLOA directions, with an effective bearing-shaft stiffness of K_{xp}, K_{yp}, K_{xg} and K_{yg} for each of the gears. The mesh stiffness is represented by K_m for the gear mesh. As before, the mesh stiffness is assumed to be time-averaged.

The excitations of the system come from the STE displacement at the gear mesh in the LOA direction and the friction force due to the sliding of mating gear

teeth in the OLOA direction. Just as in the previous section, both excitations are assumed to have constant amplitude over the entire frequency range.

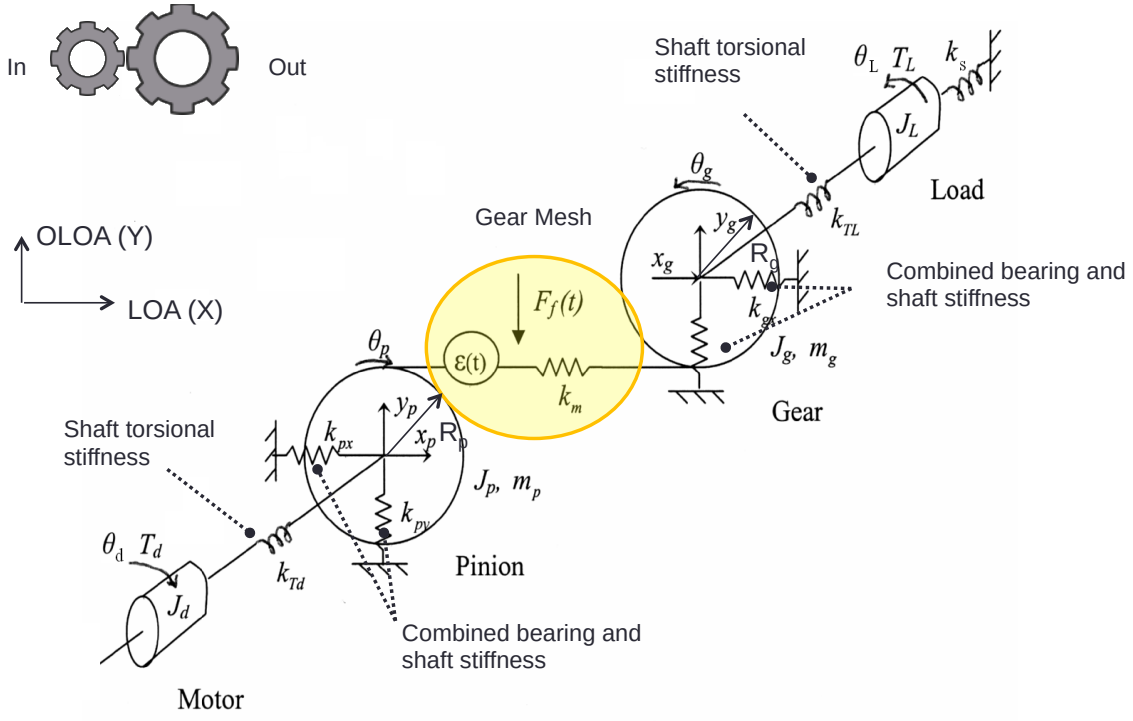

Figure 2.4: Schematic of the 8 DOF System (Model A)

Chapter 3: System Analysis

3.1 Overview and Assumptions

This section looks at how the different architectures of the two dual-mesh models compare to each other utilizing the LTI models described in Chapter 2. The responses of the two systems are used to compare the two dual-mesh architectures with each other along with the single mesh model. Some of the responses that are considered in this chapter include the natural frequencies, mode shapes, frequency spectra of the bearing forces and frequency spectra of the mesh forces. The effect of bearing stiffness, coefficient of friction, damping ratio and STE on the bearing force spectra is also explored. For each method of comparison, only a sampling of the data is shown to give an understanding of how the architectures compare to one another.

For Model A, all of the parameters are chosen to be consistent with those previously used in models of single-mesh systems [4]. These same parameters are carried over to Model B. Since the parameters being used in Model A are based on a two gear system, the parameters for the third gear in Model B are taken to be the same as the pinion in Model A. The small gear(s) in each system has 17 teeth, while the large gear(s) has 31 teeth. The mesh and bearing stiffness for the third gear, however, are reduced by 20% to allow for the differentiation of modes associated with the two gear meshes. Model C uses the same parameters as Model A for the first two gears. The third and fourth gear in Model C uses the same parameters as the second and first gear in Model A respectively. Again, the mesh stiffness and bearing stiffness for the third and fourth gear is reduced by 20% to allow for the

differentiation of modes associated with the second gear mesh. Using these choices for parameters in Models B and C allows for several useful attributes. Both Model B and C have an output speed and torque equal to its input and all three models have identical meshes between the first two gears. For all three models, a damping ratio of 0.01, a time-invariant coefficient of friction of 0.03 and a time-invariant STE of 50 μin is assumed. The complete list of parameters and their value for all three models can be found in Table 3.1.

Table 3.1: Model Parameters

Parameter	**Units**	**Model A**	**Model B**	**Model C**
First Pinion Stiffness LOA	lbf/in	82e4	82e4	82e4
First Pinion Stiffness OLOA	lbf/in	73.8e4	73.8e4	73.8e4
First Gear Stiffness LOA	lbf/in	98e4	98e4	98e4
First Gear Stiffness OLOA	lbf/in	88.2e4	88.2e4	88.2e4
Second Pinion Stiffness LOA	lbf/in			78.4e4
Second Pinion Stiffness OLOA	lbf/in			70.56e4
Second Gear Stiffness LOA	lbf/in		65.6e4	65.6e4
Second Gear Stiffness OLOA	lbf/in		59.04e4	59.04e4
First Mesh	lbf/in	2.77e6	2.77e6	2.77e6
Second Mesh	lbf/in		2.216e6	2.216e6
Driver Stiffness	lbf-in/rad	7.09	7.09	7.09
Load Stiffness	lbf-in/rad	10.08	10.08	10.08
Shaft Stiffness	lbf-in/rad			8.6

Parameter	Units	Model A	Model B	Model C
Driver Inertia	lb-in^2	1.2e-3	1.2e-3	1.2e-3
Load Inertia	lb-in^2	1.2e-3	1.2e-3	1.2e-3
First Pinion Inertia	lb-in^2	5.3e-3	5.3e-3	5.3e-3
First Gear Inertia	lb-in^2	10.6e-3	19.5e-3	19.5e-3
Second Pinion Inertia	lb-in^2			19.5e-3
Second Gear Inertia	lb-in^2		5.3e-3	5.3e-3
First Pinion Mass	lb	5.5e-3	5.5e-3	5.5e-3
First Gear Mass	lb	10.6e-3	10.6e-3	10.6e-3
Second Pinion Mass	lb			10.6e-3
Second Gear Mass	lb		5.5e-3	5.5e-3
First Pinion Radius	in	1.39	1.39	1.39
First Gear Radius	in	1.92	1.92	1.92
Second Pinion Radius	in			1.92
Second Gear Radius	in		1.39	1.39

3.2 Comparisons Among Models A, B and C

In this section the responses of the three models are considered, specifically the natural frequencies, mode shapes, dynamic bearing force and dynamic mesh force. The responses for all three models are due to two excitations, an assumed STE input of 50 μin and a friction force with a coefficient of friction of 0.03. Input and output torque fluctuations are not considered as part of these studies. Both input

excitations in this section are assumed to be time-invariant and constant. Between Models B and C, the speed reduction and transmitted torque is kept the same to allow for a comparison between the two models as they would be incorporated into an industrial system. The first mesh in Models B and C and the mesh in Model A are between gears with identical parameters to allow for a comparative view of the responses of the mesh.

3.2.1 Natural Frequencies

One of the most fundamental ways the three different models can be compared is by looking at their natural frequencies. Equation 2.9 is used for determining the natural frequency of each mode for the models. Table 3.2 shows the natural frequencies for each of the three models along with a brief description of the physical form of the mode. It can be seen that as the models increase in degrees of freedom, they keep all of the natural frequencies of the lower order models and added new modes. This is expected due to the shared parameter values among models.

Table 3.2: Natural Frequencies of Models A, B and C

Mode	Description	Model A [Hz]	Model B [Hz]	Model C [Hz]
1	Rigid body	0	0	0
2	Torsional mode			5
3	Motor torsional mode	13	13	13
4	Load torsional mode	15	16	16

Mode	Description	Model A [Hz]	Model B [Hz]	Model C [Hz]
5	Out of phase bending of second gear and pinion shaft in LOA			1216
6	Bending of second gear in OLOA			1299
7	Out of phase bending of first gear and pinion shaft in LOA	1359	1150	1359
8	Bending of first gear in OLOA	1452	1452	1452
9	In phase bending of second gear and pinion shaft in LOA		1584	1583
10	Bending of second pinion in OLOA		1649	1649
11	In phase bending of first gear and pinion shaft in LOA	1770	1769	1770
12	Bending of first pinion in OLOA	1844	1844	1844
13	Coupled torsional/bending for second mesh		6886	6887
14	Coupled torsional/bending for first mesh	7700	7700	7700

The mode shapes also provide some insight into the differences among the three systems. Figure 3.1 gives a short representation of how to read the depiction of relative motions used in this paper. The black circles with the vertical radius denote the position of the gears of the system when the system is at rest and the red circle with the radius denotes the relative motion of the gears of the system when

the system is excited at a given frequency. 3.1(a) is the initial position of the gear, 3.1(b) is the gear under a pure torsional mode, 3.1(c) is the gear under a pure translational mode in the OLOA direction and 3.1(d) is the gear under a pure translational mode in the LOA direction. For each mode, the dominant motion is taken and given a displacement of 1 radian if it is rotational or 1 unit if it is translational. All other motions of the gears are scaled compared to the dominant mode.

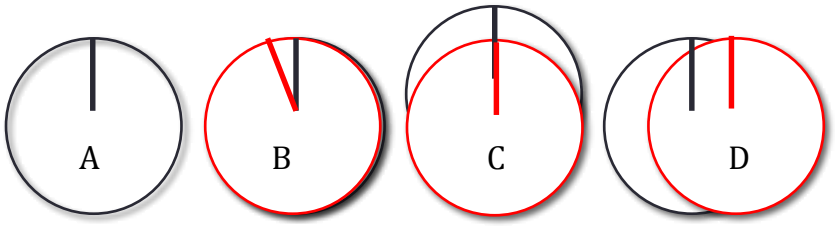

Figure 3.1: Mode Shape Representations

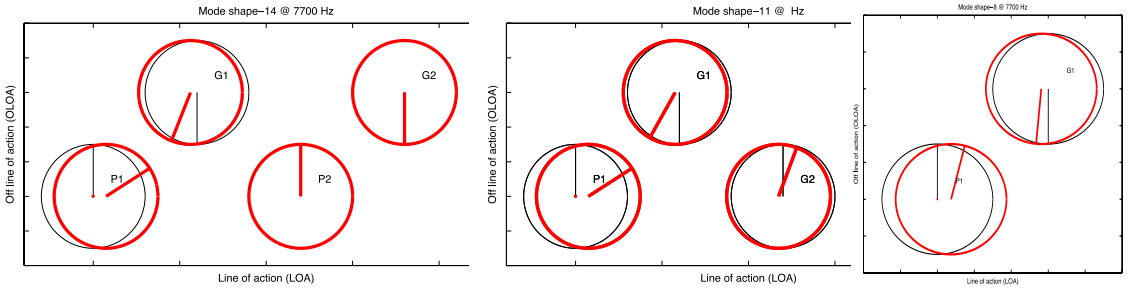

Figure 3.2: Coupled Torsional/Translational Mode for Model C (left), Model B (center) and Model A (right)

Figures 3.2 and 3.3 show the relative motions of two modes exhibited by all three of the models. The modes are chosen because they best show how the relative motions of the three models compare. In Figure 3.2, relative motions for the three models are shown for 7700 Hz. This mode corresponds to the coupled torsional/translational mode associated with the first mesh. All three models exhibit

relative motions with the first gear mesh having out of phase rotation and out of phase translation in the LOA with the exception of Model B where the third gear also exhibits in phase rotation and LOA translation with the first gear. In Model C, the third and fourth gears do not exhibit any motion.

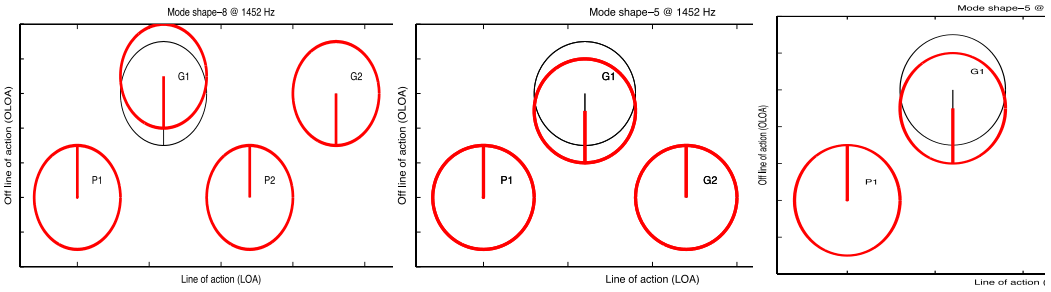

Figure 3.3: OLOA Bending Mode for Model C (left), Model B (center) and Model A (right)

Figure 3.3 shows the relative motions for the 1452 Hz mode for the three models. This mode corresponds to the off-line-of-action bending for the first gear in each system. As a contrast to the previous mode shown, this mode relates to the support structures and as a consequence, all three models exhibit similar relative motions. The first gear of each model has translational motion only in the OLOA, while all the other gears remain without motion.

3.2.2 Dynamic Bearing Force

The dynamic bearing force is of particular interest because this is where the geared system is coupled to its housing. Any force at the bearings is transmitted into the case and can potentially excite it, causing vibratory noise. The force response spectrum for the bearings on each of the three shafts in the three models is shown below as predicted by Equation 2.14. For these frequency response spectrums, each

model is excited at each gear mesh by a static transmission error of 50 μin and a sliding friction force with a coefficient of friction of 0.03. The force at each of the bearings is then predicted at each frequency over the 10 to 20,000 Hz span. Figure 3.4 shows the summation of the bearing force of each of the bearings in each model to the excitations given above. The response spectrum of Model A is the summation of the forces at the bearings of both of the gears, Model B is the summation of all three bearing forces and Model C is the summation of all four of the bearing forces. In the figure, it can be clearly seen that there are distinct resonances attributed to the bearing/shaft components of the systems and distinct resonances attributed to the gear mesh component of the systems. For each of the dual-mesh systems two peaks can be seen in the gear mesh frequency range, which is attributed to the 20% reduction of the second gear mesh stiffness. While the two dual-mesh models have similar magnitudes in their response, they are dramatically larger than the response of the single mesh model.

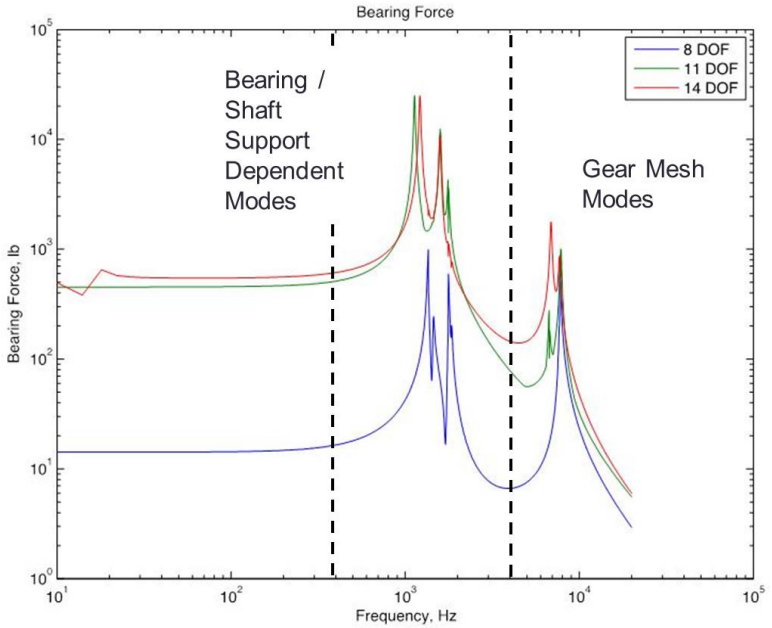

Figure 3.4: Summed Bearing Force of all Bearings for Models A (8 DOF), B (11 DOF) and C (14 DOF)

3.2.3 Dynamic Mesh Force

The next response of the models to be considered is the dynamic mesh force. The dynamic mesh force is obtained by using Equation 2.16 presented earlier. The dynamic mesh force spectrum shows how the force acting between two gears in mesh (with assumed excitation) varies over a range of frequencies, in this case 10 to 20,000 Hz. In Figure 3.5, the dynamic mesh force response spectrum is given for the first gear mesh of Models A, B and C for an STE excitation of 50 μin and a friction excitation with a coefficient of friction of 0.03. The resonances attributed to the bearing/shaft support stiffness resides in the mid frequency range and is distinct from the resonances attributed to the gear mesh which resides in the high frequency range. Across the entire frequency range considered, Models A and C exhibit similar

responses to each other. Model B exhibits similar trends to Models A and C at low and high frequencies, but has a larger magnitude around the bearing/shaft support dependent modes. Figure 3.6 gives the dynamic mesh force response spectrum for the second gear mesh for Models B and C and the gear mesh of Model A for reference. Models B and C exhibit a similar response for the dynamic mesh force response, but have a larger magnitude than the mesh force in Model A.

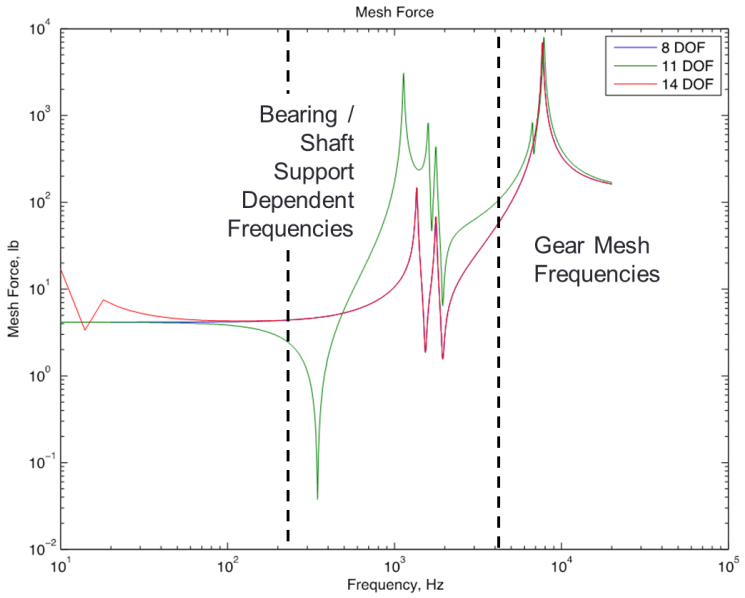

Figure 3.5: Dynamic Mesh Force of the First Gear Mesh of Models A (8 DOF), B (11 DOF) and C (14 DOF)

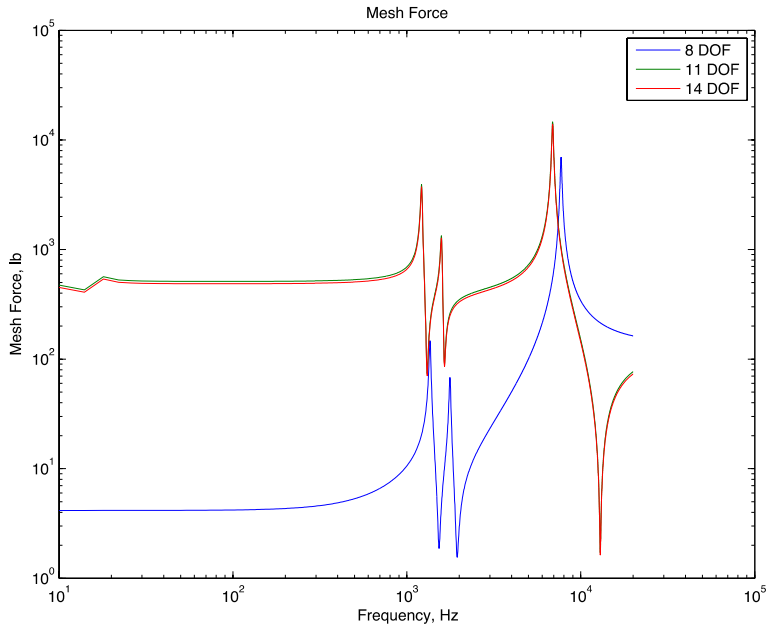

Figure 3.6: Dynamic Mesh Force of the Second Gear Mesh in Models B (11 DOF) and C (14 DOF) and the First Gear Mesh in Model A (8 DOF)

3.3 Sensitivity Studies

In addition to how the responses of the three models compare when operating under similar parameters, it can be useful to examine how each dual-mesh model behaves as various parameters are adjusted. Over the next four sections, the effect of four different parameters (static transmission error, coefficient of friction, damping ratio and bearing stiffness) on the two dual-mesh models, Models B and C, is explored in how they affect the bearing force frequency response.

3.3.1 Sensitivity to Change in STE, Coefficient of Friction and Damping Ratio

The STE and coefficient of friction directly control the magnitude of the excitation force on each of the models while the damping ratio directly controls the magnitude of all the damping elements due to how the modal damping matrix is constructed, outlined in the model formulation. Four different cases are studied for Models B and C, where in three of the cases a single parameter is increased by a multiple of five while the other two parameters remained at the nominal value used in the bearing force and mesh force studies above. The fourth case is run with all three values at the nominal level to allow for comparison to the other responses above. Table 3.3 tabulates the four cases and the values used for the STE, coefficient of friction and damping ratio for each case.

Table 3.3: Parameters Used in Sensitivity Cases

Case	μ [-]	ε [µin]	ζ [-]
I (default)	0.03	50	0.01
II	0.15	50	0.01
III	0.03	250	0.01
IV	0.03	50e	0.05

In Figure 3.7, the effect of increasing either the coefficient of friction or the STE by a multiple of five causes the same net effect on the bearing force response spectrum at the input pinion in Model B. This is expected because both excitation mechanisms cause the excitation force on the system to increase by a multiple of five as well. Increasing the damping coefficient has the opposite effect on the

system, by decreasing the magnitude of the system's resonances. A similar response to these parameter adjustments can be seen in Figure 3.8 for Model C's bearing force response spectra at the input pinion.

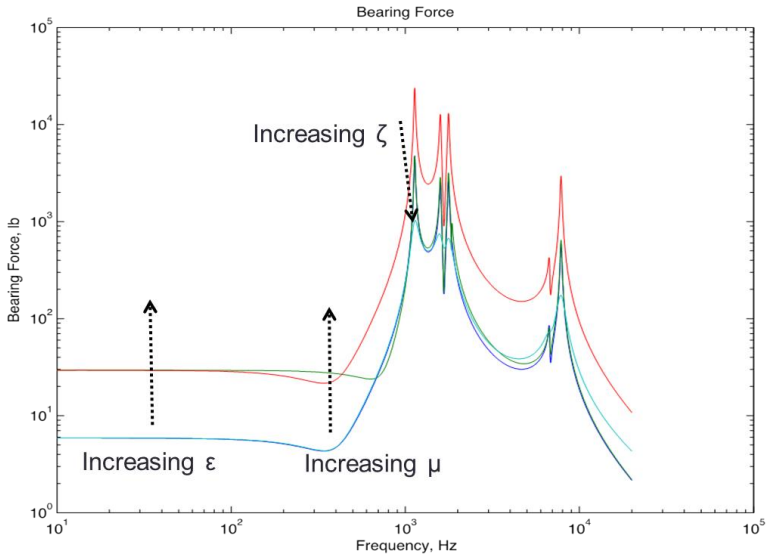

Figure 3.7: Sensitivity of Bearing Force Magnitude at Input Pinion to Change of STE, Coefficient of Friction and Damping Ratio for Model B

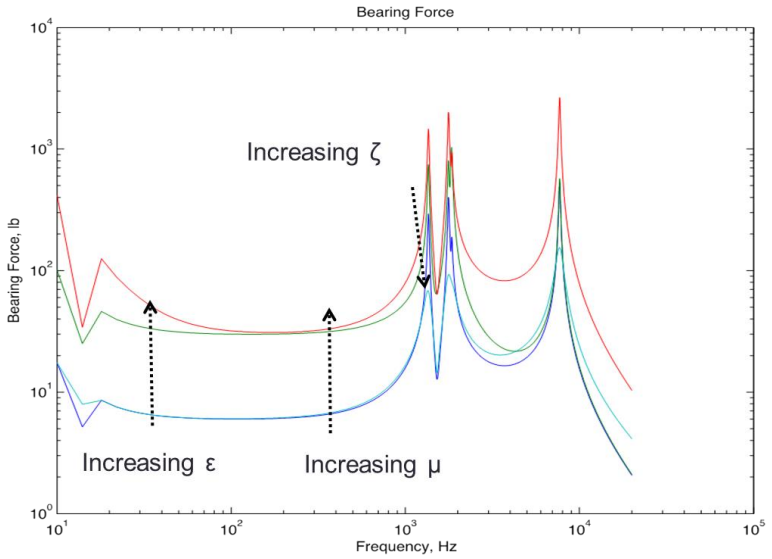

Figure 3.8: Sensitivity of Bearing Force Magnitude at Input Pinion to Change of STE, Coefficient of Friction and Damping Ratio for Model C

3.3.2 Sensitivity to Change of STE and Coefficient of Friction in LOA and OLOA

The next sensitivity to change considered is the effect of only the STE and the coefficient of friction upon the dynamic bearing force spectra at the input pinion. This time the response spectrum is considered in both the LOA and OLOA directions instead of the magnitude of the two directions. Since the sliding friction excitation acts upon the OLOA and the STE excitation acts upon the LOA, splitting the response spectrum into the OLOA and LOA directions allows for a clearer picture of how the excitations are related to the force response at the bearings. Table 3.4 gives the values used for the coefficient of friction and the STE in Models B and C during this section.

Table 3.4: Parameters Used in OLOA and LOA Sensitivity to Change Case

Case	μ [-]	ε [µin]
I (default)	0.03	50
II	0.15	50
III	0.03	250

Figure 3.9 shows the sensitivity to change of the STE and the coefficient of friction on the LOA and OLOA bearing force response spectrum at the first pinion in Model B. In the LOA direction, increasing either the STE or coefficient of friction by a multiple of five results in an increase of the bearing force response by the same amount. In the OLOA direction, only increasing the coefficient of friction has an effect on the bearing force response spectrum, resulting in an increase in magnitude. Any change in the STE has no effect on the bearing force response in the OLOA

direction. A similar trend can be seen in Figure 3.10 where the sensitivity to change of the static transmission error and the coefficient of friction on the LOA and OLOA bearing force response spectrum at the first pinion in Model C is shown.

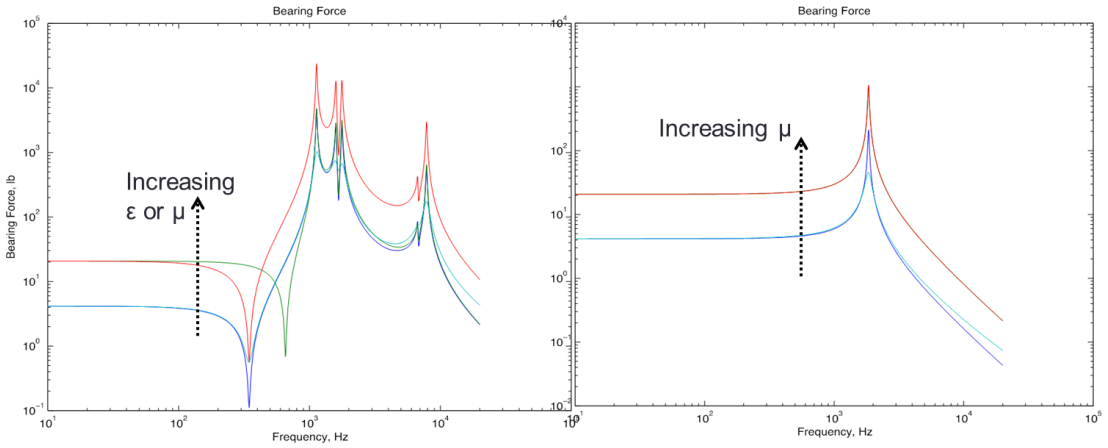

Figure 3.9: Sensitivity of Bearing Force at Input Pinion to Change of STE and Coefficient in LOA (left) and OLOA (right) Directions for Model B

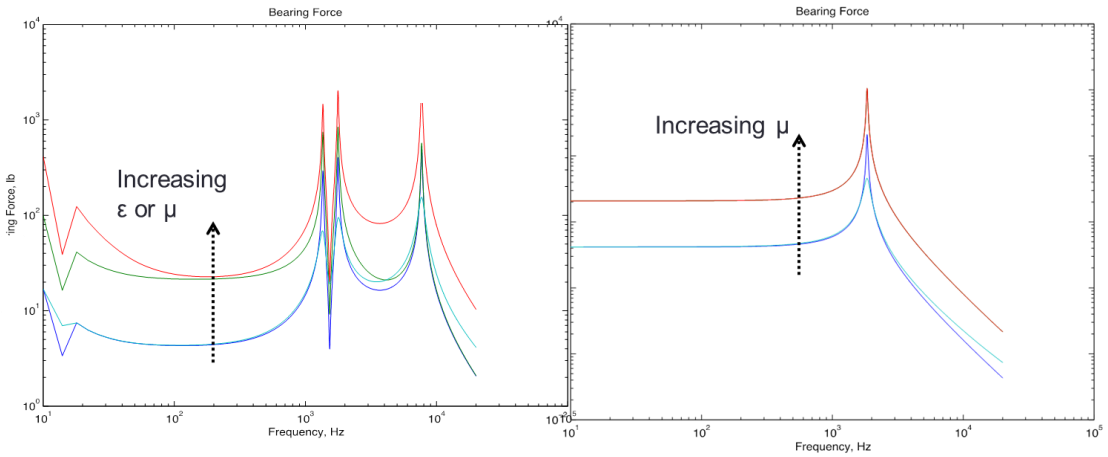

Figure 3.10: Sensitivity of Bearing Force at Input Pinion to Change of STE and Coefficient in LOA (left) and OLOA (right) Directions for Model C

3.3.3 Effect of Varying Coefficient of Friction Between Meshes

It is common for dual-mesh gear systems to have different coefficients of friction at different gear meshes due to manufacturing deviations, wear and other factors. This section looks at the effect of having a different coefficient of friction between the gear meshes in Models B and C in four cases. Case I uses the default value for the coefficient of friction as described in Section 3.2 for both meshes. Case II assumes the coefficient of friction associated with the first gear mesh is increased by a multiple of five while the second mesh remains at its default value, and Case III assumes the coefficient of friction for the second gear mesh is increased by a multiple of five while the first mesh remains at its default value. Case IV assumes the coefficient of friction at both meshes is increased by a multiple of five from the default value. Table 3.5 helps illustrate the values used in each of the cases.

Table 3.5: Parameters Used in Varying Coefficient of Friction Between Meshes

Case	1st Mesh μ [-]	2nd Mesh μ [-]
I (Default)	0.03	0.03
II	0.15	0.03
III	0.03	0.15
IV	0.15	0.15

The results of the four cases can been seen in Figure 3.11 for the bearing force response spectrum for Model B. Case II and IV resulted in the same effect, an increase in magnitude over the low frequency range (below the shaft/support dependent frequencies) while having minimal increase in magnitude at mid/high

frequencies. Case III, however, had minimal effect on the bearing force response. Figure 3.12 shows the results of the same four cases for Model C. Here cases II and IV have the same effect, an increase in magnitude of the bearing force response over the entire frequency range, and Case III has minimal effect on the bearing force response.

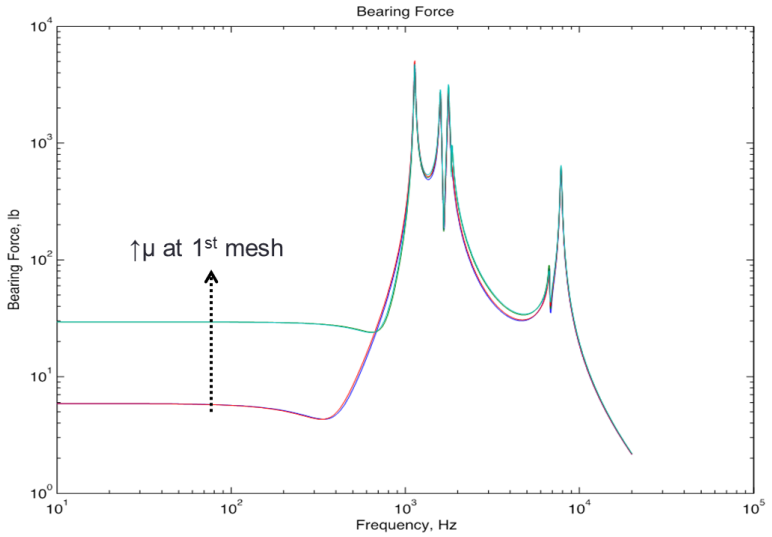

Figure 3.11: Effect on Bearing Force Magnitude at Input Pinion to Varying Coefficient of Friction Between Meshes on Model B

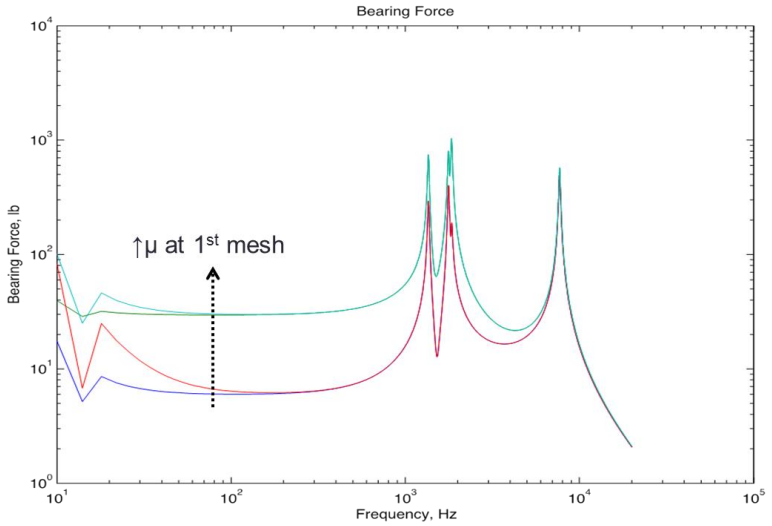

Figure 3.12: Effect on Bearing Force Magnitude at Input Pinion to Varying Coefficient of Friction Between Meshes on Model C

3.3.4 Sensitivity to Bearing Stiffness

A sensitivity study is conducted with Models B and C to see how changing the bearing stiffness affects the bearing force response spectrum over the 10 to 20,000 Hz range. Three cases are conducted for each model. Case II uses the nominal values for the bearing stiffness (lumped with the shaft support stiffness) as described in Section 3.2. For Case I, the bearing stiffness at each bearing location in Models B and C is decreased by 20% from the nominal value, and for Case III, the bearing stiffness at each bearing location in Models B and C is increased by 20% from the nominal value. Table 3.5 illustrates the values being used in the three cases.

Table 3.6: Parameters for Sensitivity to Change of Bearing Stiffness

	Case I	Case II	Case III
Bearing Stiffness Parameters	$0.8k_x$ $0.8k_y$	k_x k_y	$1.2k_x$ $1.2k_y$

The effect of changing the bearing stiffness on the bearing force response spectrum for Model B is shown in Figure 3.13. Increasing the bearing stiffness shifts the associated modes to higher frequencies. The gear mesh resonances are not affected by a change in bearing stiffness. In Figure 3.14 a similar trend can be observed for Model C.

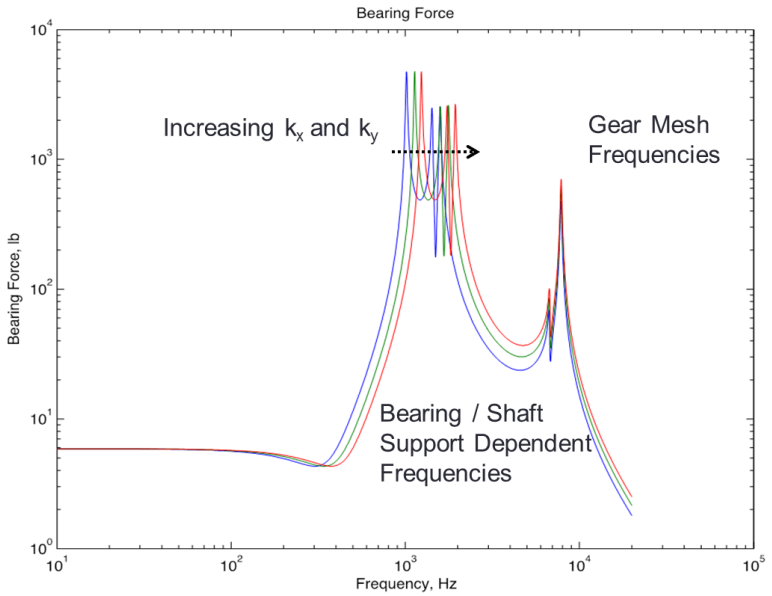

Figure 3.13: Sensitivity to Change of Bearing Stiffness on First (Input) Shaft for Model B

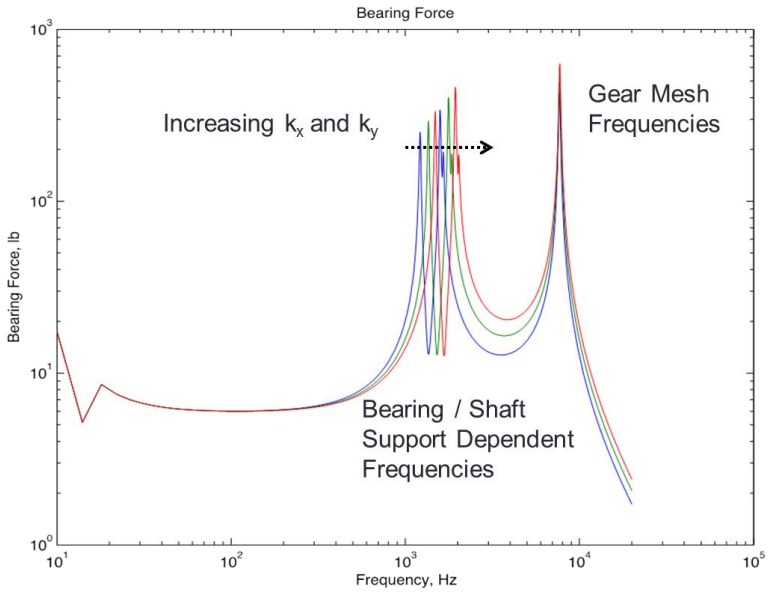

Figure 3.14: Sensitivity to Change of Bearing Stiffness on First (Input) Shaft for Model C

Chapter 4: Conclusions

4.1 Summary

In this thesis, LTI analytical models for two dual-mesh systems, Models B and C, are developed in the frequency domain. Compared with a single mesh model, Model A, these conceptual models are used to understand how the dynamic system responses change due to changes in system parameters and assumed excitations (STE in LOA and sliding friction in OLOA). For the three models, the natural frequencies and mode shapes are calculated and classified. In each model, similar shapes are observed at mesh frequencies as well as rigid body frequencies. Differences are observed in associated bearing/shaft support modes. The higher DOF models have additional modes in this range, as expected. When considering the summation of the force spectrum at each bearing (with assumed input the meshes), the multi-mesh models exhibit higher bearing loads than the single mesh. A similar trend is observed on the calculated dynamic mesh force spectra. An increase in the excitations (sliding friction or STE) or a decrease in damping enhances bearing forces at the input pinion (for both Models B and C). Sliding friction or STE affects the LOA bearing force while only sliding friction affects the OLOA (in both Models B and C). Change in sliding friction at the first mesh (input side) has a major effect on bearing force magnitude at the input pinion in the low frequency range (below bearing/shaft support modes) for both models. Model B shows more sensitivity to changes in sliding friction at the first mesh near the bearing/shaft support modes than Model C. Change in sliding friction at second mesh (output side) has minimal

effect on bearing forces at the input bearing for both models. Increases in bearing stiffness shifts the associated modes to higher frequencies, as expected.

4.2 Limitations of Model and Sources of Error

The analytical model developed in this study has several limitations. Firstly, the model is time invariant. In real world systems, the excitations and stiffness are time dependent on gear position and change throughout the rotation of the gears. Creating a time variant model would reflect real world systems more closely. Second, the damping coefficients are determined by modal damping, which is a reasonable approximation but is not always accurate. In addition, this is a conceptual model, so it is useful to obtain some understanding of how a geared system behaves, but it is not able to accurately predict the system response (forces or motions).

There are a few sources of error present in this model. When determining the effect of varying the bearing stiffness, the same STE is used in all three cases. The contacts mechanics program that is used to determine the STE value factors in bearing stiffness into its calculation. By varying the bearing stiffness a new STE should have been used but this study is looking at the effect of bearing stiffness with holding all other variables constant. In addition, the physical parameters of the gear system are taken from a previous study, so the precision and the manner that these measurements were taken is not known.

4.3 Extensions of Models

Extensions to the conceptual models proposed will increase their complexity as well as require many more parameters to be calculated or measured. Linear time variant (LTV) models can be formulated and compared to the LTI models to determine what additional insights can be gained with more model complexity. The current LTI and future LTV models can be extended to a vibro-acoustic model, to calculate radiated sound pressure, by incorporating a transfer function that relates the bearing loads to the radiated sound pressure level. These transfer functions can be empirical or generated using a combination of finite element (for relationship between bearing load and casing structure motions) and boundary element (for relationship between casing structure motions and radiated sound pressure levels) models. Other multi-mesh gearing configurations, such as planetary, or different gearing types, such as helical, spiral bevel, or hypoid, can be also formulated.

References

[1] D. Houser and R. Singh, Gear Dynamics and Gear Noise, Short Course Notes (sections on Basic Gear Dynamics by R. Singh, on CD, 2013).

[2] J. Lin, R. G. Parker, Mesh stiffness vibration in-stabilities in two-stage gear systems, Journal of Vibration and Acoustics 124 (2002) 68–76.

[3] Load Distribution Program (LDP), Windows 3.3.0 version, Gear and Power Transmission Research Lab, The Ohio State University (2009).

[4] Holub, Allison, Mobility Analysis of a Spur Gear Pair and the Examination of Sliding Friction, The Ohio State University (2005).

[5] Srinivasan, Vijay, Mobility Analysis of Structure-Borne Noise Paths in a Simplified Rotorcraft Gearbox System, The Ohio State University (2010).

List of Symbols and Abbreviations

Symbols

ε : Static Transmission Error

μ : Coefficient of Friction

ξ : Damping Ratio

n : Number of Degrees of Freedom

l : Moment Arm

ω : Natural Frequency

M : Mass Matrix

C : Damping Ratio Matrix

K : Stiffness Matrix

F : Force Vector

Q : Eigenvector Matrix

q : Motion Vector

F_{STE} : Force due to Static Transmission Error

F_r : Force due to Sliding Friction

F_{px} : Line-Of-Action Dynamic Bearing Force of Pinion

F_{py} : Off-Line-Of-Action Dynamic Bearing Force of Pinion

F_p : Dynamic Bearing Force of Pinion

F_m : Dynamic Mesh Force

k_m : Mesh Stiffness

c_m : Mesh Damping

J_L : Inertia of Load

J_d : Inertia of Driver

k_{TL} : Torsional Stiffness of Load

k_{Td} : Torsional Stiffness of Driver

k_T : Torsional Stiffness of Shaft

x_i : Line-Of-Action Translational Motion of the i^{th} Gear

y_i : Off-Line-Of-Action Translational Motion of the i^{th} Gear

θ_i : Torsional Motion of the i^{th} Gear

J_i : Inertia of the ith Gear

R_i : Radius of the ith Gear

m_i : Mass of the ith Gear

k_{ix} : Line-Of-Action Stiffness of the ith Bearing/Shaft

k_{iy} : Off-Line-Of-Action Stiffness of the ith Bearing/Shaft

c_{ix} : Line-Of-Action Damping of the ith Bearing/Shaft

c_{iy} : Off-Line-Of-Action Damping of the ith Bearing/Shaft

Abbreviations

LOA : Line of Action

OLOA : Off Line of Action

LTI : Linear Time Invariant

DOF : Degrees of Freedom

DTE : Dynamic Transmission Error

DMF : Dynamic Mesh Force